

Investigation of Three-Dimensional Upward and Downward Directed Gas-Liquid Two-Phase Bubbly Flows in a 180°-Bent Tube

Th. Frank, R. Lechner, F. Menter

CFX Development, ANSYS Germany GmbH, Staudenfeldweg 12,
D-83624 Otterfing, Germany
Thomas.Frank@ansys.com

Abstract

Upward and downward directed disperse bubbly flows through horizontal pipeline and 180° pipe bend have been predicted using the Eulerian multiphase flow model of CFX-5 (CFX, 2004) and taking into account Grace drag, Tomiyama lift, Tomiyama wall lubrication and FAD turbulent dispersion forces (see Frank et al., 2004). Starting from the investigation of the single phase water flow using SST and algebraic Reynolds stress (EARSM) turbulence models, good agreement between the CFD solution and the experimental data provided by Takamasa & Kondo (1995) could be obtained for the primary and secondary single phase fluid motion in the pipe bend. Further upward and downward directed gas-liquid two-phase flows have been predicted using the CFX-5 multiphase flow model. The results were compared to the measured gas volume fraction distributions in five defined measurement cross sections C1-C5 in the pipe bend. Again the numerical results were found in qualitatively good agreement with the experimental data published by Takamasa & Kondo (1995) showing the applicability and level of accuracy of the multiphase flow models for disperse bubbly flows in complex geometries.

Keywords

CFD, curved duct, gas-liquid flow, disperse bubbly flow, non-drag forces, turbulence

1. Introduction

Gas-liquid two-phase flows in straight pipes and in curved ducts are commonly found in industrial plants such as chemical and nuclear reactors, boilers and heat exchangers. But most experimental and numerical studies of gas-liquid two-phase flows carried out in the past by many authors were focused on flow regimes in straight vertical pipes only, e.g. Serizawa (1987), Tomiyama (1998) and Prasser (2003). Due to the absence of pronounced secondary flows in the carrier liquid phase the flow regimes and quasi steady-state gas volume fraction distributions in vertical pipe flows are determined by one-dimensional force balances between gravity, drag and buoyancy forces in vertical direction and lift, turbulent dispersion and wall forces in the horizontal direction. The presence of secondary flow in a curved, C- or U-shaped 180°-bent pipe causes more complicated interaction between the two phases than occur in straight pipelines. Such kind of dedicated three-dimensional flows are therefore better suited to reveal still existing deficiencies of existing two-phase Eulerian models for disperse bubbly flows.

2. The Experiments

This study is based on experimental work on upward and downward directed gas-liquid bubbly flows in C-shaped pipes carried out by Usui et.al. (1980/81), Takamasa & Kondo (1995) and Takamasa & Tomiyama (1999). In the experiments carried out by Takamasa & Kondo (1995) a disperse bubbly flow with prescribed superficial air and water velocities enters a horizontal pipe of 28mm inner diameter. After a horizontal pipe section of 60D the flow enters a 180° C-shaped pipe bend with 125mm bend radius followed by another horizontal pipe section of 60D. Both upward and downward flows had been investigated experimentally. The apparatus used in the experiments by Takamasa & Kondo (1995) is illustrated in Fig. 1, while the schematic setup showing the geometrical dimensions of the flow geometry under consideration and the location of the measurement cross sections is indicated on the right of Fig. 1. The fluids in the experiments entered the pipe and C-shaped bend at near to atmospheric pressure. The water temperature was maintained at a level of $20 \pm 0.5^\circ\text{C}$. For the injection of the gaseous phase a bubble generator consisting of four sintered (porous) brass tubes with a particle-passing diameter of $1.5 \mu\text{m}$ was used. From the applied stereo image-processing methodology the resulting bubble diameter was determined to be $d_p=4\text{mm}$ under the given flow conditions.

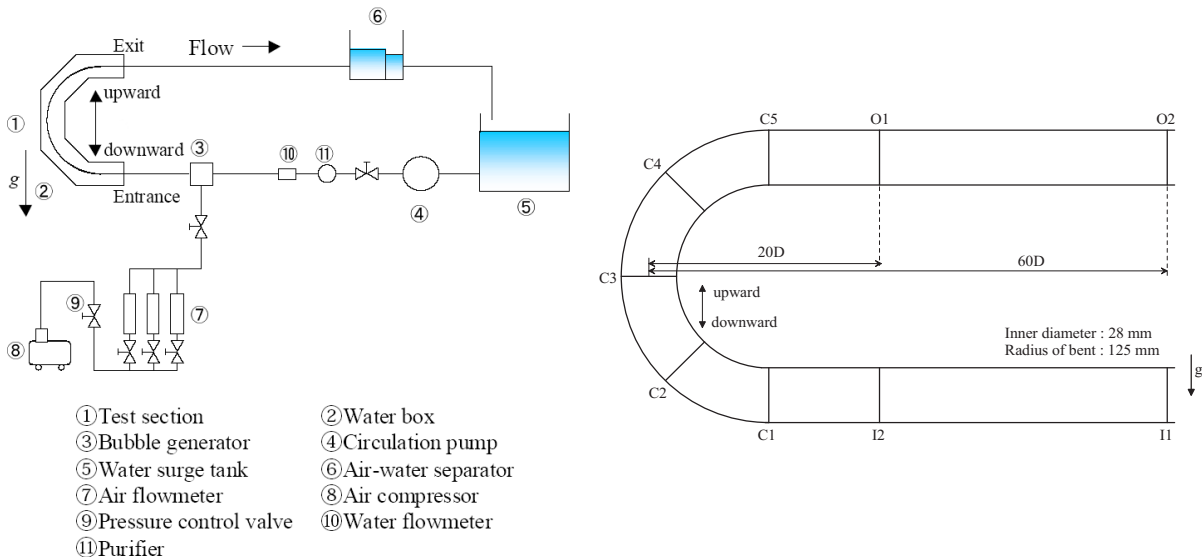


Figure 1: Experimental apparatus (side view) for the investigation of upward and downward gas-liquid flows through pipe bends as used by Takamasa & Kondo (1995). Schematic view on the right shows geometrical dimensions and measurement locations of water velocity profile and void fraction distribution measurements

In the experiments, the water and air superficial velocities were varied from $j_L=0.71$ to 1.79 m/s and $j_G=0.027$ to 0.0135 m/s, respectively. Due to the limited availability of published experimental data the superficial water and air velocities of $j_L=1.43\text{m/s}$ and $j_G=0.0135\text{m/s}$ were selected for the intended experiment vs. CFD prediction comparison, resulting in a gas-liquid flow of about 1% averaged gas void fraction. The comparison with the flow maps established by Usui et al. (1980/81) for upward and downward directed gas-liquid flows through pipe bends show, that the investigated gas-liquid multiphase flow is well in the regime of diluted bubbly flow (see Fig. 2). In the experiments liquid velocities in the flow direction (primary flow) and the tube diametric direction (secondary flow) were measured using an LDV. From the published data of Takamasa & Kondo (1995) and Takamasa & Tomiyama (1999) corresponding water velocity profiles from the LDV

measurements are available in 5 different pipe cross sections C1-C5 in the pipe bend at 0°, 45°, 90°, 135° and 180° (see Fig. 1). Additionally a Stereo Imaging Methodology using CCD camera had been applied to the gas-liquid flow. Gas void fraction distributions in cross sections C1-C5 had been determined from the measured bubble locations and bubble diameter distributions for both upward and downward flows.

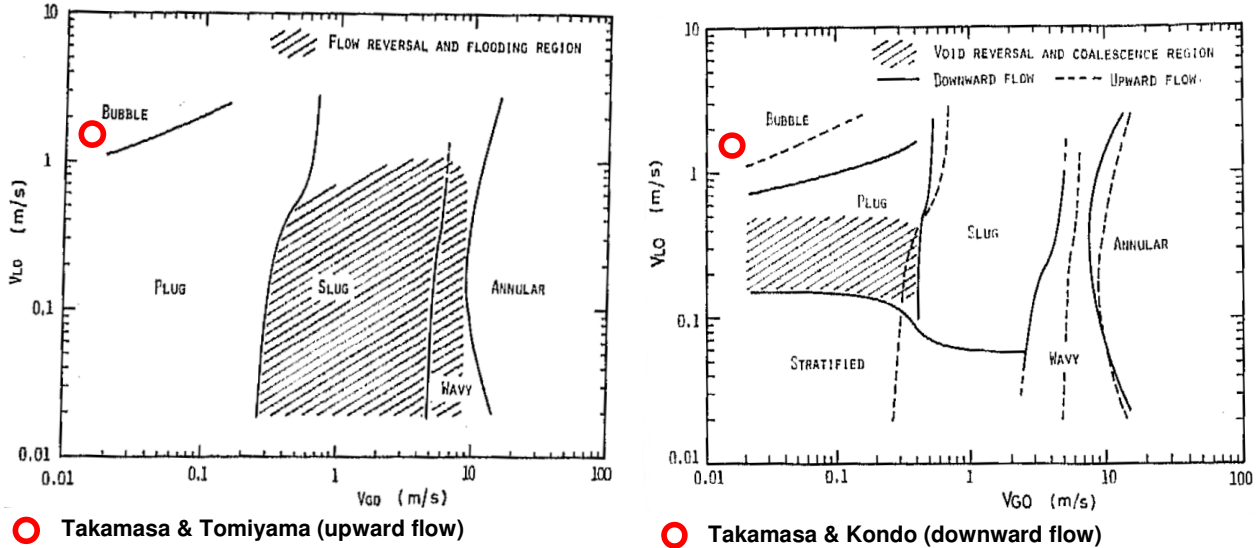


Figure 2: Flow regime maps for upward (left) and downward (right) directed gas-liquid flows in pipe bends as investigated by Usui et al. (1980/81); comparison of investigated flow conditions with respect to varying flow regimes in dependence on gas and water superficial velocities.

3. CFD Calculations – The Numerical Model

3.1. Numerical Mesh and Boundary Conditions

The flow geometry shown in Fig. 1 has been modeled with a numerical mesh of about 410.000 hexahedral mesh elements using ICEM/CFD. In order to reduce the overall mesh size and computational effort flow symmetry in the vertical plane has been assumed. The resulting semicircular pipe cross section was resolved in the numerical simulations by 1736 mesh elements, while 236 mesh elements were distributed along the pipe. The dimensionless wall distance of the wall nearest grid element was thereby evaluated to be about $y^+ \sim 10-22$. For the prescribed water and air superficial velocities $j_L = 1.43$ m/s and $j_G = 0.0135$ m/s the corresponding single phase flow Reynolds number was $Re \sim 45.000$. Pipe walls have been treated as hydrodynamically smooth walls. Homogeneous inlet conditions corresponding to the given superficial velocities have been assigned to the I1 cross section for upward flow and to O2 cross section for downward flow. As indicated by the measurements of Takamasa & Kondo (1995) a constant mean bubble diameter of $d_p = 4$ mm was assumed for the disperse phase. An average static pressure outlet boundary condition has been applied to O2 or I1 cross section respectively for upward or downward flow. Simulations were carried out under steady state conditions.

3.2. Single Phase Flow Turbulence Modeling

In the present study the flow through the pipe bend was simulated using the commercial CFD package CFX-5.7 (CFX, 2004). Since the gas-liquid flow mainly depends on the accurate prediction of the turbulent flow in the pipe bend and the developing secondary flows, a first aim of this validation study was the detailed comparison of CFX single phase flow predictions to the

experimental LDV data for primary and secondary flow water velocity profiles in C1-C5 cross sections as provided by Takamasa & Tomiyama (1995).

Two different turbulence models are used for this study. The first is the well known Shear Stress Transport (SST) turbulence model derived by Menter (1994) with automatic wall treatment. The second model is an explicit algebraic Reynolds stress model (EARSM). The implementation is based on an EARSM, which has recently been published by Hellsten (2004). This model in turn is based on an EARSM formulated by Wallin and Johansson (2000). Like the SST model it combines the $k-\omega$ model of Wilcox for the inner region of a boundary layer with the standard $k-\epsilon$ model in the outer wake region. The SST and EARSM models differ however in the computation of the Reynolds stress tensor. Standard two-equation turbulence models usually use the eddy viscosity concept, where the Reynolds stresses are computed as the product of an eddy viscosity and the mean strain-rate tensor, in other words the Reynolds stresses are linearly related to the mean strain-rate tensor. The eddy viscosity is then approximated as the product of a constant coefficient C_μ , a turbulent velocity scale v_T and a turbulent length scale l_T . The SST turbulence model also relies on the linear stress-strain relation, but the computation of the turbulent viscosity has been modified in order to account for the transport of the turbulent shear stress and depends on the second invariant of the mean strain-rate tensor. This can be interpreted as a variable coefficient C_μ and gives improved results in adverse pressure gradient and separated flows.

The explicit algebraic Reynolds stress model does not use the eddy viscosity concept. It has been derived from the Reynolds stress transport equation and gives a nonlinear relation between the Reynolds stresses $\overline{u_i u_j}$ and the mean strain-rate and vorticity tensors of the following form:

$$\overline{u_i u_j} = k(a_{ij} + 2/3\delta_{ij}) \quad (1)$$

where the anisotropy tensor a_{ij} is expressed using the following tensor polynomial:

$$\begin{aligned} a_{ij} = & \beta_1 S_{ij} + \beta_3 \left(\Omega_{ik} \Omega_{kj} - \frac{1}{3} II_\Omega \delta_{ij} \right) + \beta_4 \left(S_{ik} \Omega_{kj} - \Omega_{ik} S_{kj} \right) + \\ & \beta_6 \left(S_{ik} \Omega_{kl} \Omega_{lj} + \Omega_{ik} \Omega_{kl} S_{lj} - \frac{2}{3} IV \delta_{ij} \right) + \\ & \beta_9 \left(\Omega_{ik} S_{kl} \Omega_{lm} \Omega_{mj} - \Omega_{ik} \Omega_{kl} S_{lm} \Omega_{mj} \right) \end{aligned} \quad (2)$$

S_{ij} and Ω_{ij} denote the non-dimensional strain-rate and vorticity tensors, respectively. The tensor invariants are given by:

$$II_\Omega = \Omega_{kl} \Omega_{lk} \quad , \quad IV = S_{kl} \Omega_{lm} \Omega_{mk} \quad (3)$$

The calculation of the β -coefficients is more complex and beyond the scope of this paper. Details can be found in Hellsten (2004). Due to the higher order terms in equation (2) many flow phenomena such as secondary flows and streamline curvature are included in the model without the need to solve the full Reynolds stress transport equations.

3.3 The Eulerian Gas-Liquid Flow Model

The simulation of the gas-liquid dispersed bubbly flow is based on the CFX-5.7 two-fluid (or multifluid) Euler-Euler approach (CFX, 2004). The Eulerian modeling framework is based on ensemble-averaged mass and momentum transport equations for all phases. Regarding the liquid phase as continuum ($\alpha=L$) and the gaseous phase (bubbles) as disperse phase ($\alpha=G$) with a constant bubble diameter d_p these equations without mass transfer between phases read:

$$\frac{\partial}{\partial t}(r_\alpha \rho_\alpha) + \nabla \cdot (r_\alpha \rho_\alpha \vec{U}_\alpha) = 0 \quad (4)$$

$$\frac{\partial}{\partial t}(r_\alpha \rho_\alpha \vec{U}_\alpha) + \nabla \cdot (r_\alpha \rho_\alpha \vec{U}_\alpha \otimes \vec{U}_\alpha) = \nabla \cdot (r_\alpha \mu_\alpha (\nabla \vec{U}_\alpha + (\nabla \vec{U}_\alpha)^T)) - r_\alpha \nabla p + r_\alpha \rho_\alpha \vec{g} + \vec{F}_D + \vec{M}_\alpha \quad (5)$$

where r_α , ρ_α , μ_α are the void fraction, density and viscosity of the phase α and M_α represents the sum of interfacial forces besides the drag force F_D , like lift force F_L , wall lubrication force F_{WL} and turbulent dispersion force F_{TD} . For the steady state investigations within the scope of this paper it had been proven that the virtual mass force F_{VM} is small in comparison with the other non-drag forces and therefore it can be safely neglected. As described in the previous chapter turbulence of the liquid phase has been modeled using either Menter's $k-\omega$ based Shear Stress Transport (SST) model or an algebraic Reynolds stress transport model (EARSM). Due to the small differences encountered between the SST and EARSM models for the single phase flow predictions (see 4.1.), all following gas-liquid two-phase flow simulations were carried out with the SST turbulence model. The turbulence of the disperse bubbly phase was modeled using a zero equation turbulence model and bubble induced turbulence has been taken into account according to Sato (1975). The drag force between the bubbles and the fluid was considered in the distorted bubble regime according to the Grace drag model build into CFX-5. The lift force was calculated according to Tomiyama (1998):

$$\vec{F}_L = C_L r_G \rho_L (\vec{U}_L - \vec{U}_G) \times \nabla \times \vec{U}_L \quad (6)$$

Tomiyama (1998) has performed extensive investigations of the lift force coefficient C_L for disperse bubbly flows. For an air-water two-phase flow he has found a changing sign of C_L depending on the bubble size diameter at about $d_p = 5.8$ mm:

$$C_L = \begin{cases} \min[0.288 \tanh(0.121 \text{Re}_p), f(Eo_d)], & Eo_d < 4 \\ f(Eo_d), & 4 \leq Eo_d \leq 10 \\ -0.27, & Eo_d > 10 \end{cases} \quad (7)$$

with:

$$f(Eo_d) = 0.00105 Eo_d^3 - 0.0159 Eo_d^2 - 0.0204 Eo_d + 0.474 \quad (8)$$

where Eo_d is the Eötvös number based on the long axis d_H of a deformable bubble, i.e.:

$$Eo_d = \frac{g(\rho_L - \rho_G)d_H^2}{\sigma}, \quad d_H = d_p(1 + 0.163 Eo)^{1/3}, \quad Eo = \frac{g(\rho_L - \rho_G)d_p^2}{\sigma} \quad (9)$$

Antal et al. (1991) proposed an additional wall lubrication force to model the repulsive force of a wall on a bubble, which is caused by the asymmetric fluid flow around bubbles in the vicinity of the wall due to the fluid boundary layer. Within the present model we take into account this wall force in the modified formulation of Tomiyama (1998):

$$\vec{F}_{WL} = -C_{WL} r_G \rho_L \left| \vec{U}_{rel} - (\vec{U}_{rel} \cdot \vec{n}_W) \vec{n}_W \right|^2 \vec{n}_W \quad (10)$$

where the wall lubrication force coefficient has been determined by Tomiyama (1998) based on experiments with air bubbles in glycerin:

$$C_{WL} = C_{W3} \frac{d_p}{2} \left(\frac{1}{y_w^2} - \frac{1}{(D - y_w)^2} \right) \quad (11)$$

where the coefficient C_{W3} is dependent on the Eötvös number for deformable bubbles:

$$C_{W3} = \begin{cases} e^{-0.933Eo+0.179} & 1 \leq Eo \leq 5 \\ 0.00599Eo - 0.0187 & 5 < Eo \leq 33 \\ 0.179 & 33 < Eo \end{cases} \quad (12)$$

with \vec{n}_w as the normal vector to the wall, d_p as the bubble diameter, \vec{U}_{rel} as the velocity difference between the phases and r_G as the gas volume fraction. In contrary to Antal et al. (1991), Tomiyama proposed an inverse quadratic proportionality of this force with respect to the wall distance y . The turbulent dispersion force can be derived from a Favre average of the interfacial drag force (see Burns et al. 2004, Frank et al. 2004) and is calculated for a two-phase flow according to:

$$\vec{F}_{TD,\alpha} = D_{\alpha\beta} A_{\alpha\beta} \frac{\nu_{t\alpha}}{\sigma_{r\alpha}} \left(\frac{\nabla r_\beta}{r_\beta} - \frac{\nabla r_\alpha}{r_\alpha} \right) \quad (13)$$

with $A_{\alpha\beta} = 6r_\beta/d_\beta$ being the interfacial area density for a continuous phase α and a disperse phase β , $\nu_{t\alpha}$ the turbulent eddy viscosity of the continuous phase and $\sigma_{r\alpha}$ a turbulent Schmidt number, for which a default value of 0.9 has been used for the presented flow predictions. Finally for a two-phase disperse bubbly flow ($r_\alpha + r_\beta = 1$; $\nabla r_\alpha + \nabla r_\beta = 0$) the Favre Averaged Drag (FAD) turbulent dispersion force acting on the disperse phase can be written as:

$$\vec{F}_{TD} = -C_D \frac{3\nu_{t\alpha}\rho_\alpha}{4\sigma_{r\alpha}d_p} \frac{1}{1-r_\beta} |U_\alpha - U_\beta| \nabla r_\beta \quad (14)$$

The given non-drag force models were implemented in CFX-5 and are available since the code version CFX-5.7 (see Frank et. al 2004). Using User FORTRAN for the prediction of the various force coefficients other drag and non-drag force models can be implemented as well.

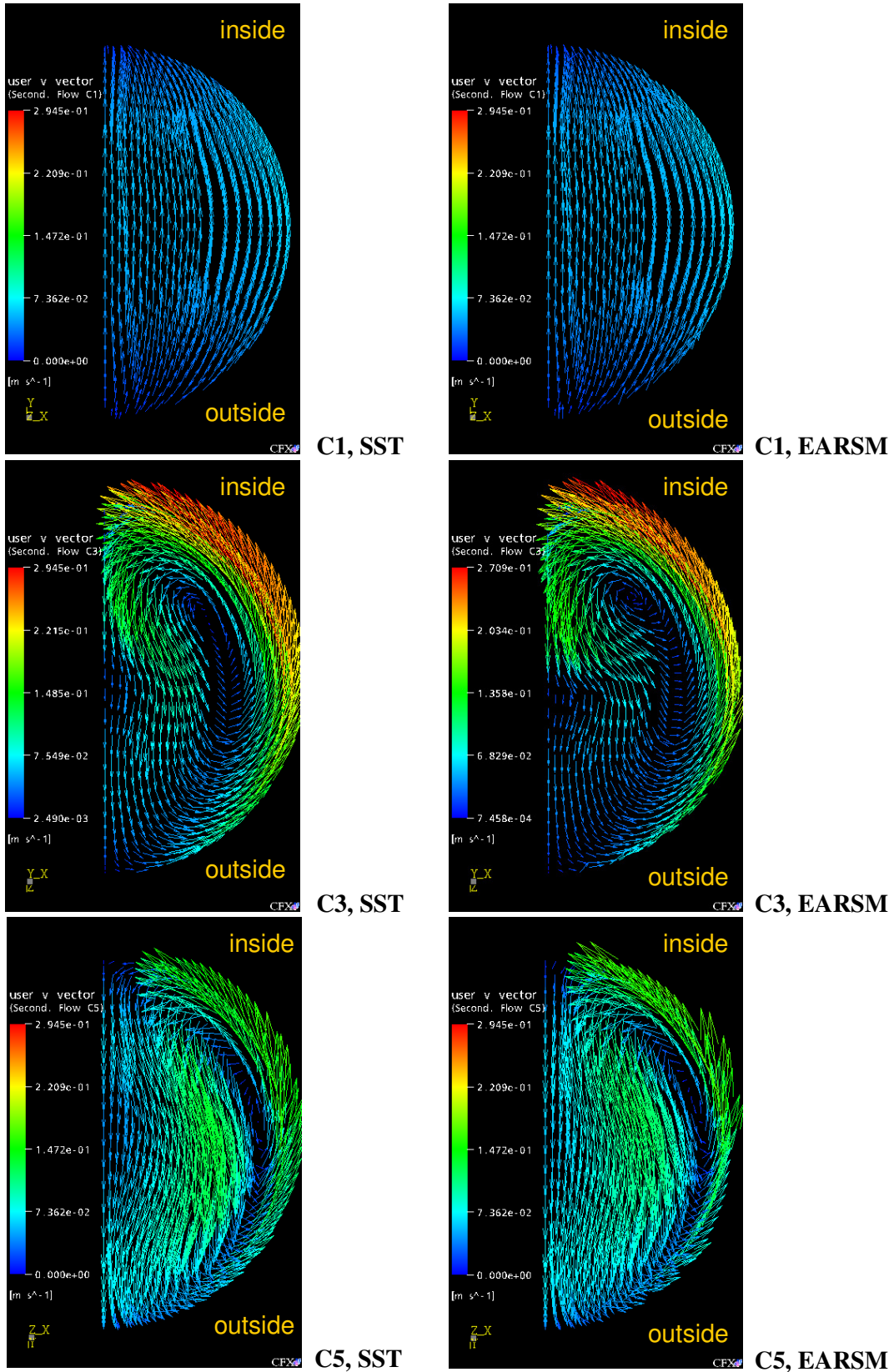


Figure 3: Secondary flows in C1, C3 and C5 pipe bend cross sections as predicted for single phase water flow with CFX-5 using the SST and EARSM turbulence models.

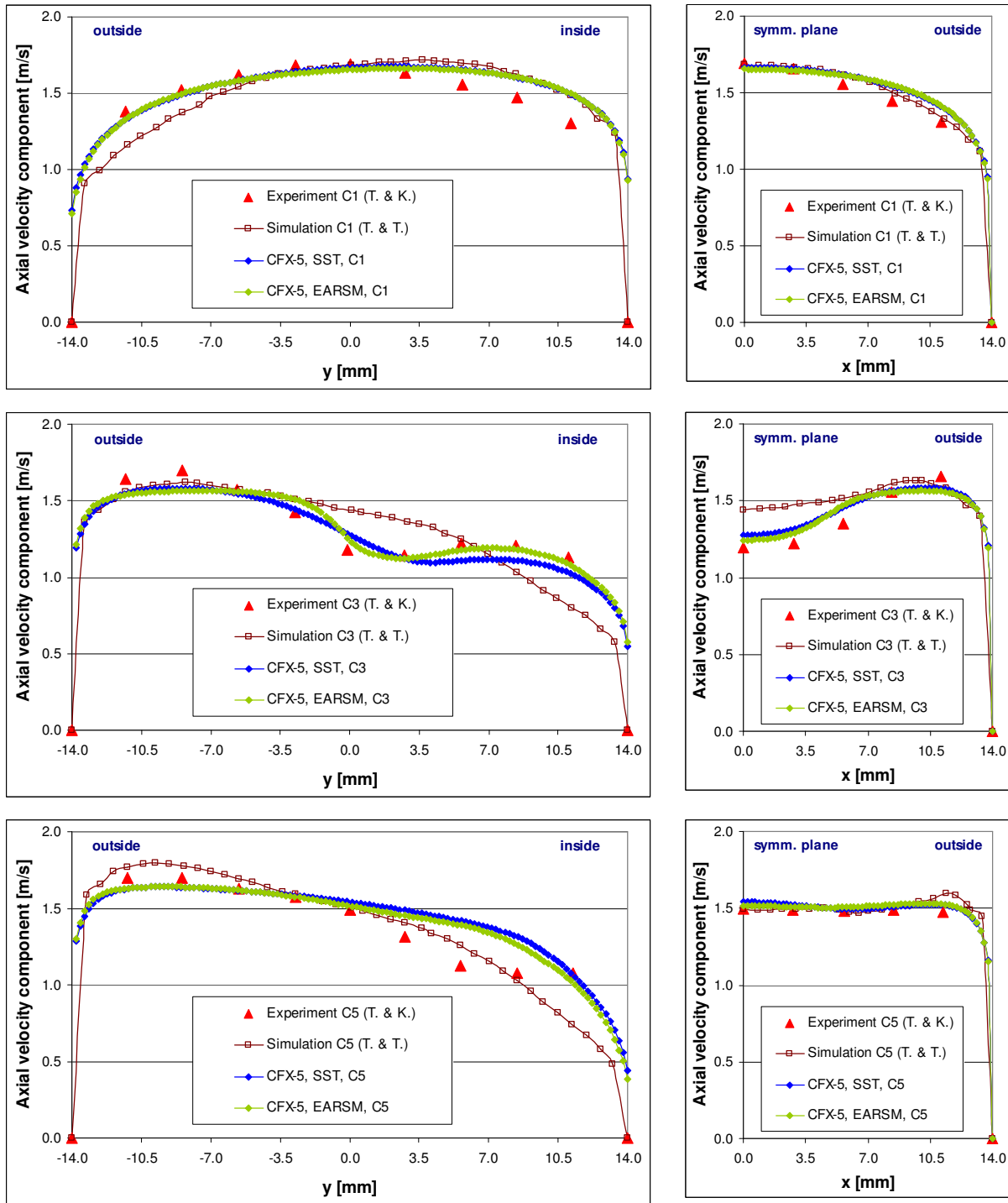


Figure 4: Primary flow profiles for the C1, C3 and C5 cross sections for single phase water flow. Comparison of CFX-5 predictions with experiments of Takamasa & Kondo (1995) and simulation results of Takamasa & Tomiyama (1999).

4. Results and Comparison to Experimental Data

4.1. Upward Directed Liquid Single-Phase Flow

In a first study the development of upward directed single phase water flow ($j_L=1.43$ m/s, $j_G=0.0$ m/s) along the pipe and 180° bend has been numerically investigated and the results obtained with the SST and EARSM turbulence models have been compared to the experiments of Takamasa & Kondo (1995) as well as to the numerical predictions of Takamasa & Tomiyama (1999). Fig. 3 shows the predicted secondary flows. In the figure, the left hand shows results obtained with the SST model and the right hand, results obtained with the EARSM algebraic Reynolds stress turbulence model. The profiles were confirmed to be almost symmetric in the experiments of Takamasa & Kondo (1995), so that the symmetry assumption considered for the numerical simulations was satisfied.

The single phase water flow enters the 180° pipe bend with an almost developed turbulent velocity profile and negligible secondary flows as shown in Fig. 3 for cross section C1. The X-axis is the horizontal spanwise axis in the cross sections, pointing from the symmetry plane towards the pipe wall, while the Y-axes mark the symmetry axes of the cross sections C1-C5. Due to the acceleration of the fluid at the inside of the bend and corresponding pressure differences across the pipe cross section, relatively high secondary flow has been developed at the 90-degree point. Secondary flow is directed from the inside wall toward the outside of the bend along the Y-axis. A counter flow from the outside toward the inside wall along the tube side wall can be observed. While the SST and EARSM solutions in the C1 and C5 cross section are almost identical, small differences between both solutions with respect to the location of the secondary flow vortex center and its intensity can be observed for the C3 cross section.

Fig. 4 shows the water velocity profiles of the primary flow, i.e. axial velocity component profiles at C1, C3 and C5 bend cross sections. The profiles at the bend inflow cross section C1 show only small deviation from a fully developed turbulent velocity profile, also slightly higher water velocities are predicted at the inside wall of the pipe. At the 90-degree point (C3) primary flow shows a changed axial velocity distribution with distinctly higher water velocities near the outside pipe wall and a remarkable lower velocity level near the inside wall of the pipe bend. Both SST and EARSM turbulence models are able to predict the axial velocity profiles in good agreement with the measurements, also the accuracy of the algebraic Reynolds stress model seems to be even slightly better. The axial velocity maximum observable at the C3 cross section is then flattening out again in the C5 cross section in both the X- and Y-axes directions. The secondary flow from the outside toward the inside wall (Fig. 3), along the tube side wall, travel counter to the high-velocity primary flow near the outside wall of the bend (Fig. 4). The fluid velocity profile at the O2 cross section after $L\sim 55D$ shows again an almost developed turbulent velocity profile.

4.2. Upward Directed Gas-Liquid Flow

Taking the predicted single phase water flow as a starting point, the upward directed gas-liquid disperse bubbly flow with $j_L=1.43$ m/s and $j_G=0.0135$ m/s was predicted. Unfortunately no detailed velocity or volume fraction profile data are provided by Takamasa & Tomiyama (1999), so the comparison between numerical simulation and experiments is limited to the provided qualitative volume fraction distributions in the measurement cross sections C1-C5. Fig. 5 shows the distribution of higher gas volume fraction for the bubbly flow under investigation. Initially bubbles are uniformly distributed over the pipe cross section at the inlet. After $L\sim 7D$ the disperse bubbly phase is completely demixed due to buoyancy and forms a region of higher gas volume fraction at the top of the horizontal pipe. Inside the bend bubbles travel near the inside wall of the bent tube due to centrifugal force and the bubble motion seems not very much affected by secondary fluid motion.

After the 180-degree point (C5) the gaseous phase is again demixing and crosses the pipe cross section towards the upper pipe wall (see Fig. 6). The onset of this second phase separation process in the CFX-5 numerical predictions seems to be delayed by a small axial distance of about 1-2D in comparison to the experiments of Takamasa & Kondo (1995), while the separation starts too early (inside the bend) and is almost finished at the C5 cross section in the numerical predictions of Takamasa & Tomiyama (1999). This can be observed in Fig. 6 and by comparison of the experimentally obtained and numerically predicted gas volume fraction profiles shown for the defined measurement cross sections C1-C5 at Fig. 7. In the paper of Takamasa & Tomiyama (1999) it is supposed, that strong secondary flow in the upper half of the pipe bend may have had an effect on the bubble shape and consequently on the bubble interfacial drag too. Therefore the observed sensitivity in the numerical simulations with respect to the location of onset of the secondary phase separation behind the bend can probably be explained by small differences in bubble drag.

4.3. Downward Directed Gas-Liquid Flow

Finally the downward directed gas-liquid bubbly flow was simulated under the same flow conditions with $j_L=1.43$ m/s and $j_G=0.0135$ m/s. Again shortly behind the inlet cross section the gaseous phase is almost completely demixed from the liquid phase due to buoyancy and the flow enters the pipe bend with highest gas volume fractions at the upper and therefore outer wall of the horizontal pipe. Both, the developing secondary fluid flow and the centrifugal force are now acting on the gaseous phase and lead to a shift of the bubbles towards the inner wall of the pipe bend. As can be seen from Fig. 8 bubbles reach the inner wall of the pipe bend approximately at the C3-C2 cross section (approx. at the 135-degree point). The gas volume fraction distributions predicted by CFX-5 are qualitatively in a very good agreement with the corresponding measurements of Takamasa & Kondo (1995). Note, that for the experiments the cross-sections C1-C5 are named in counter-clockwise order for downward flow.

As an interesting detail it can be observed, that gas volume fractions in the C3 cross section are significantly less than 1.5% near the symmetry plane of the geometry. The same effect can be seen from the isosurface representation of gas volume fraction in the pipe bend in Fig. 9. Gas bubbles obviously reach higher volume fraction in the vortex cores of the secondary fluid motion due to centrifugal force effects. Additionally higher velocities of the secondary fluid motion in the symmetry plane lead to dilution of the gaseous phase at this location.

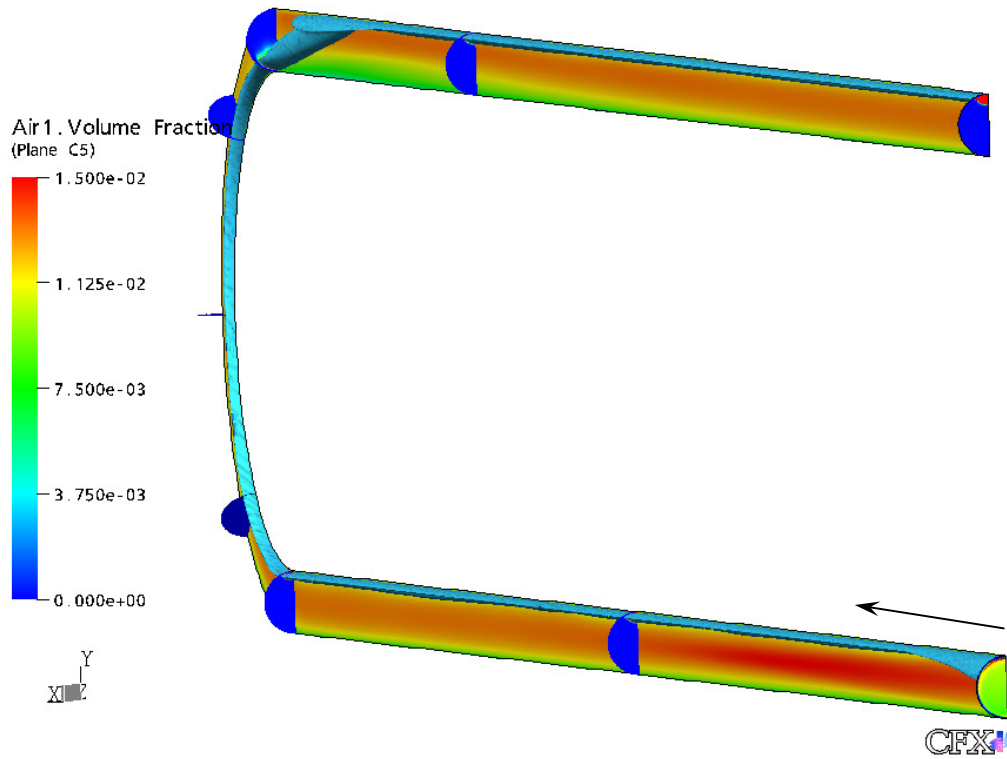


Figure 5: Isosurface of 1.5% gas volume fraction in upward gas-liquid two-phase flow through 180° pipe bend.

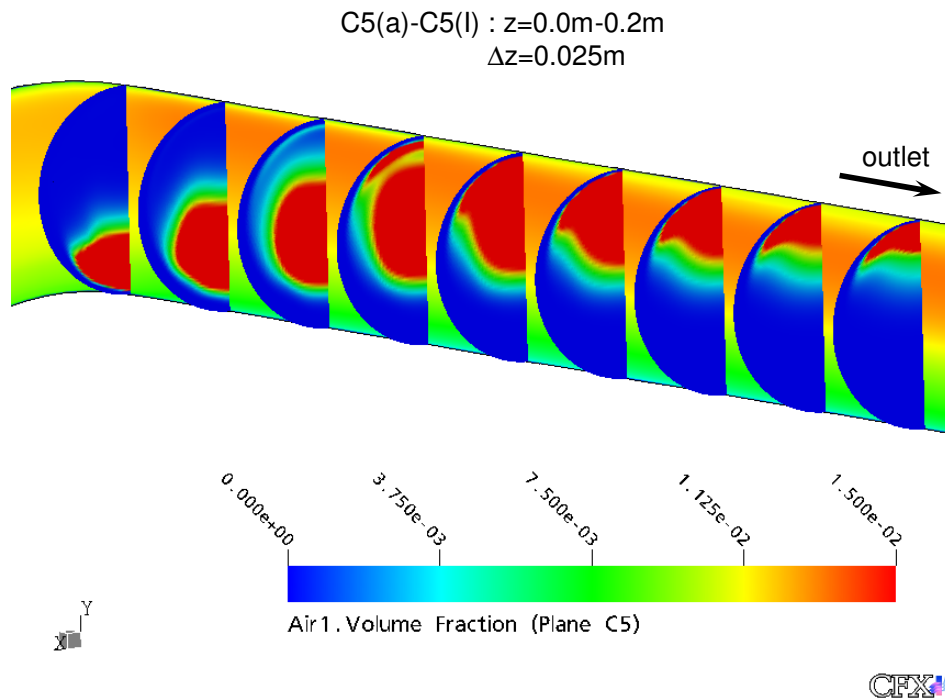
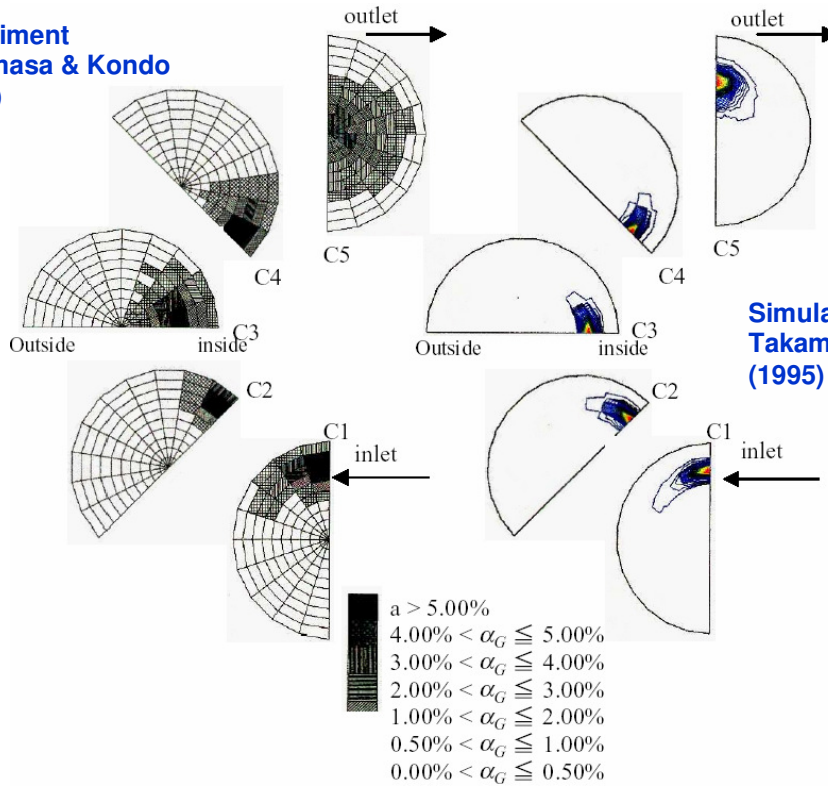


Figure 6: Re-separation of bubbles in the upper horizontal pipeline after passing cross section C5 in upward directed two-phase flow behind the C-shaped pipe bend.

Experiment
Takamasa & Kondo
(1995)



CFX-5 Simulation

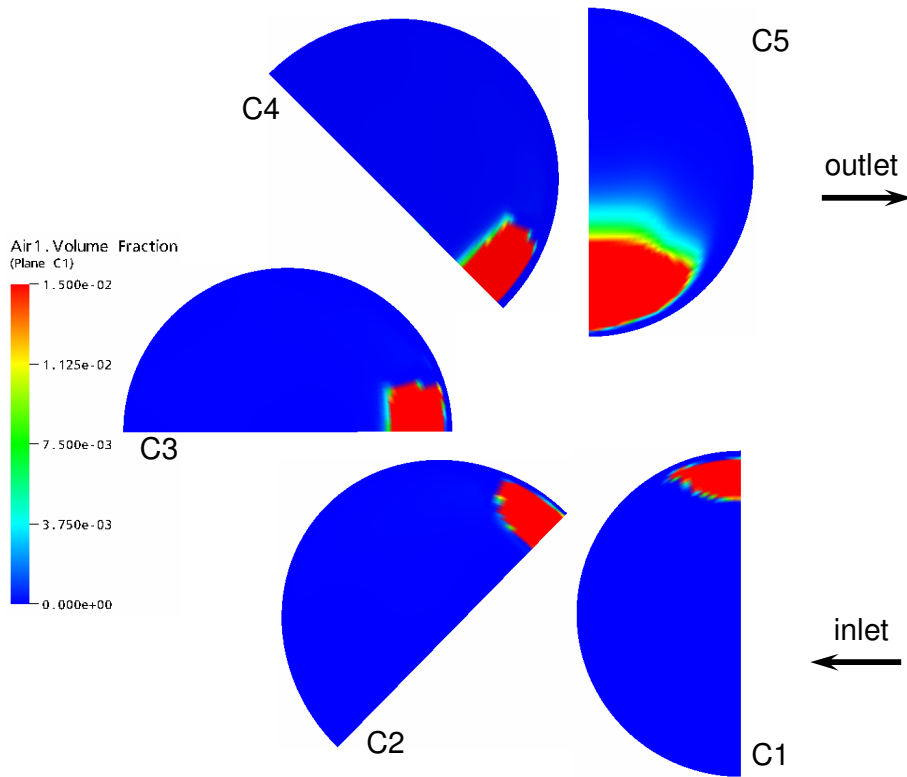
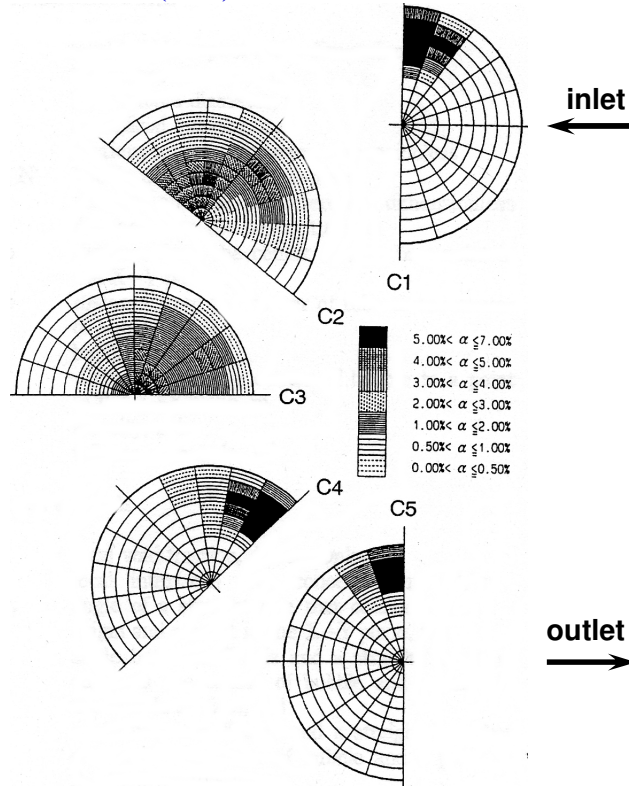


Figure 7: Comparison of gas volume fraction profiles at measurement locations C1-C5 of the Takamasa & Kondo (1995) experiments for upward directed gas-liquid flow.

Experiment Takamasa & Kondo (1995)



CFX-5 Simulation

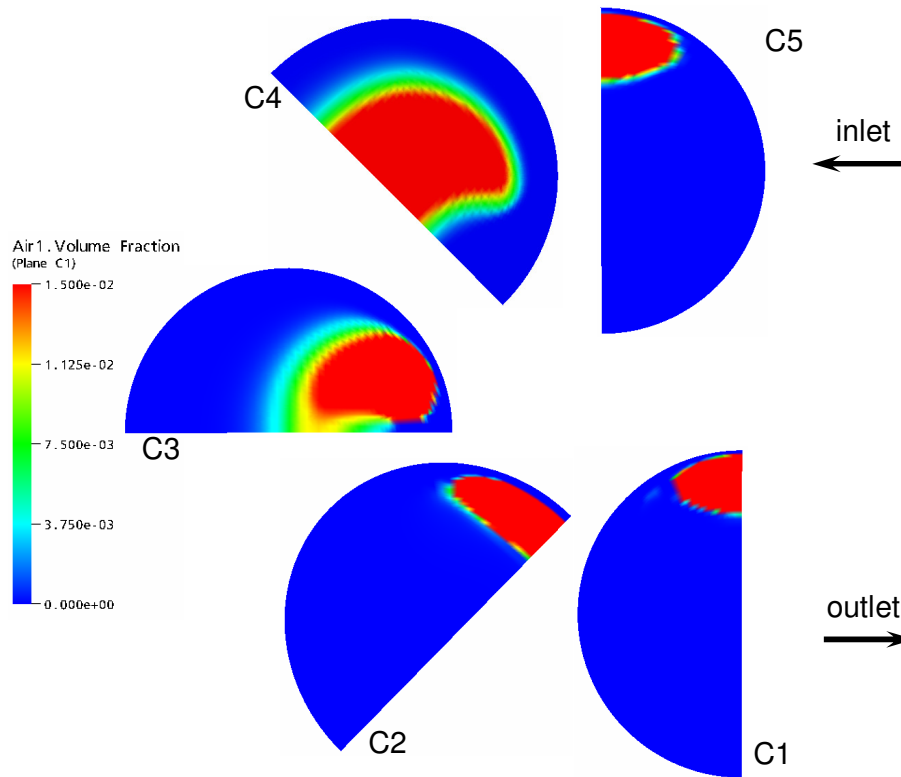


Figure 8: Comparison of gas volume fraction profiles at measurement locations C1-C5 of the Takamasa & Kondo (1995) experiments for downward directed gas-liquid flow. Note the different naming convention for the C1-C5 cross sections here.

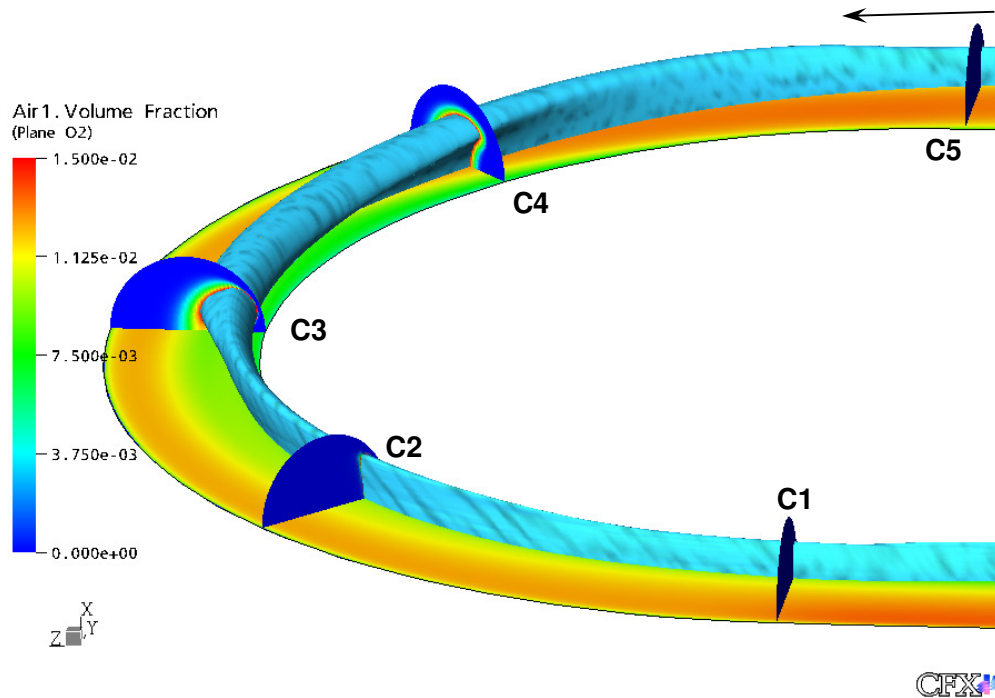


Figure 9: Isosurface of 1.5% gas volume fraction in downward directed gas-liquid two-phase flow through 180° pipe bend.

Summary and Conclusions

Upward and downward directed disperse bubbly flows through horizontal pipeline and 180° pipe bend have been predicted using the Eulerian multiphase flow model of CFX-5 and taking into account Tomiyama lift, Tomiyama wall lubrication and FAD turbulent dispersion forces. Starting from the investigation of the single phase water flow using SST and algebraic Reynolds stress (EARSM) turbulence models, good agreement between CFD solution and experimental data could be obtained for the primary and secondary fluid motion in the pipe bend. It was found that the use of the EARSM algebraic Reynolds stress turbulence model led only to a minor increased accuracy in the prediction of the fluid secondary vortex flow in the pipe bend in comparison with the SST model. For the gas-liquid two-phase flow it was observed from both experimental and numerical investigations that in the upward flow the gaseous phase travels along the inside wall of the bend due to centrifugal force. The separation of bubbles to the upper wall of the horizontal pipe section starts only behind the C5 measurement cross section. Whereas for the downward flow it was found, that the bubbles are entering the pipe bend on the upper pipe wall and travel towards the inner pipe bend wall already within the first 90° of the pipe bend and reach the pipe bend inner wall shortly after the C3 and before the C2 cross section due to centrifugal force and secondary flows developing in the liquid phase. The gas void fraction distributions in C1-C5 pipe bend cross sections have been compared to the measurements. Again the numerical results were found in qualitatively good agreement with the experimental data published by Takamasa & Kondo (1995).

Acknowledgement

This research has been supported by the German Ministry of Economy and Labour (BMWA) in the framework of the German CFD Network on Nuclear Reactor Safety Research.

References

1. Antal S.P., Lahey R.T., Flaherty J.E.: Analysis of phase distribution in fully developed laminar bubbly two-phase flow, *Int. J. Multiphase Flow*, Vol. 17, 635-652, 1991.
2. Burns A.D., Frank T., Hamill I., Shi J.-M.: The Favre averaged drag model for turbulence dispersion in Eulerian multi-phase flows, *5th Int. Conf. on Multiphase Flow, ICMF'2004*, Yokohama, Japan, 2004.
3. CFX-5.7 User Manual, ANSYS-CFX, 2004.
4. Frank Th., Shi J., Burns A.D.: Validation of Eulerian multiphase flow models for nuclear reactor safety applications, *3rd International Symposium on Two-phase Flow Modeling and Instrumentation*, Pisa, 22.-24. Sept. 2004
5. Hellsten A.: New advanced $k-\omega$ turbulence model for high-lift aerodynamics, *AIAA Paper 2004-1120*, Reno, Nevada, 2004.
6. Menter F.R.: Two-equation eddy-viscosity turbulence models for engineering applications, *AIAA-Journal*, Vol. 32, No. 8, 1994.
7. Prasser H.-M. et al.: Strömungskarten und Modelle für transiente Zweiphasenströmungen, *Wissenschaftlich-Technische Berichte, FZR-379*, Forschungszentrum Rossendorf, Germany, Juni 2003.
8. Sato Y., Sekoguchi K.: Liquid velocity distribution in two phase bubble flow, *Int. J. Multiphase Flow*, Vol. 2, pp. 79-95, 1975.
9. Serizawa A., Kataoka I.: Phase Distribution in Two-Phase Flow, *Proc. ICMHT Int. Seminar on Transient Phenomenon in Multiphase Flow*, Dubrovnik, 1987.
10. Takamasa T., Kondo K.: Measurement of interfacial configurations on bubbly flow in 180°-bend tube using image-processing method, *Transactions Japan Soc. Mech. Eng.*, Vol. 61, pp. 16-22, July 1995 (in Japanese).
11. Takamasa T., Kondo K.: Measurement of Bubble Motion in Bend Tube using Image-Processing Method, *ANS Proc. Of the Nat. Heat Transfer Conference*, HTC-Vol. 8, pp. 110-117, Portland, Oregon, USA, August 5-9, 1995.
12. Takamasa T., Tomiyama A.: Three-Dimensional Gas-Liquid Two-Phase Bubbly Flow in a C-Shaped Tube, *9. Int. Topical Meeting on Nuclear Reactor Thermal Hydraulics (NURETH-9)*, San Francisco, California, USA, October 3-8, 1999.
13. Tomiyama A.: Struggle with Computational Bubble Dynamics, *Third Int. Conf. On Multiphase Flow, ICMF'98*, Lyon, France, June 8-12, 1998.
14. Usui K., Aoki S., Inuoe A.: Flow Behavior and Pressure Drop of Two-Phase Flow through C-Shaped Bend in Vertical Plane (I – Upward Flow), *J. Nucl. Science and Technology*, Vol. 17, No. 12, pp. 875-887, 1980.
15. Usui K., Aoki S., Inoue A.: Flow behavior and pressure drop of two-phase flow through C-shaped bend in vertical plane (II – Downward flow), *J. Nucl. Science and Technology*, Vol. 18, No. 3, pp. 179-190, 1981.
16. Wallin S., Johansson A.: Modeling streamline curvature effects in explicit algebraic Reynolds stress turbulence models, *International journal of Heat and Fluid Flow*, 23(5), pp. 721-730, 2002.